Materials and Design 190 (2020) 108562

Contents lists available at ScienceDirect

Materials and Design

journal homepage: www.elsevier.com/locate/matdes

Synthesis of alkali-silica reaction product structurally identical to that formed in field concrete

Zhenguo Shi [a,*], Andreas Leemann [a], Daniel Rentsch [b], Barbara Lothenbach [a,c]

[a] Laboratory for Concrete & Construction Chemistry, Swiss Federal Laboratories for Materials Science and Technology (Empa), 8600 Dübendorf, Switzerland
[b] Laboratory for Functional Polymers, Swiss Federal Laboratories for Materials Science and Technology (Empa), 8600 Dübendorf, Switzerland
[c] Department of Structural Engineering, Norwegian University of Science and Technology (NTNU), 7491 Trondheim, Norway

HIGHLIGHTS

- Alkali-silica reaction product structurally identical to that formed in field concrete is synthesized.
- Formation of 12.0 Å, 10.8 Å and 13.1 Å alkali-silica reaction products is found to be related to the reaction temperature.
- Swelling of the crystalline alkali-silica reaction products cannot be the mechanism that causes expansion of concrete.

GRAPHICAL ABSTRACT

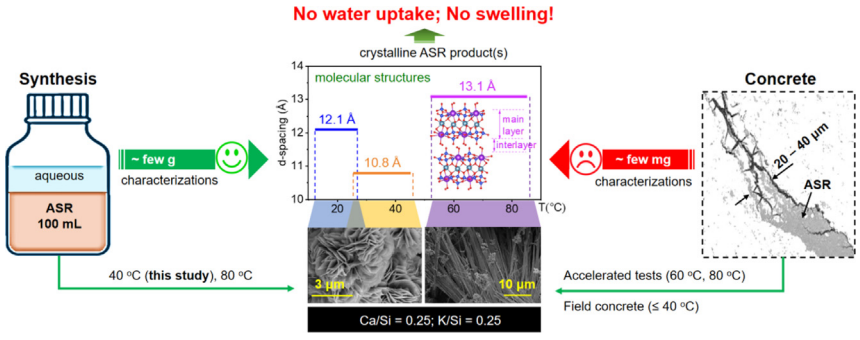

ARTICLE INFO

Article history:
Received 3 December 2019
Received in revised form 26 January 2020
Accepted 8 February 2020
Available online 8 February 2020

Keywords:
Alkali-silica reaction
Synthesis
K-shlykovite
Crystal structure
Concrete

ABSTRACT

Alkali-silica reaction (ASR) can cause expansion and cracking of concrete. Despite significant progress over the past 80 years, the molecular structures of the ASR products remain poorly understood. These reaction products are present in very small amounts within concrete aggregates, which severely limit their chemical and physical characterizations. In this study, synthesis of an ASR product structurally identical to that formed in field concrete is achieved in large quantities at 40 °C. The temperature is found to affect the formation of different types of crystalline ASR products: 12.0 Å (<40 °C), 10.8 Å (around 40 °C), and 13.1 Å (60–80 °C for K-shlykovite), which all have layered silicate-sheet structures. Both 10.8 and 13.1 Å ASR products cannot swell at high relative humidity. This suggests that swelling of the studied crystalline ASR products by uptake of water cannot be the mechanism of ASR-induced expansion at 40 to 80 °C. These findings help to better understand ASR in concrete and pave the way for developing innovative solutions for limiting ASR.

1. Introduction

Concrete, which is made by mixing cement and aggregates with water, plays a vital role in modern civilization. It is the second most

* Corresponding author.
E-mail address: zhenguo.shi@empa.ch (Z. Shi).

https://doi.org/10.1016/j.matdes.2020.108562

consumed material on a global scale after water. However, aggregates (which typically account for 60 to 75% of the total volume of concrete) can sometime react with alkalis from the concrete pore solution to form alkali-silica reaction (ASR) products. These products can subsequently cause expansion and cracking of concrete and significantly shorten the service life of concrete infrastructures [1]. Aggregates reactive in the presence of alkalis have been reported across almost all the continents [2–5]. Using such alkali-reactive aggregates is inevitable due to the globally increased demand of aggregates. In 2019, the world demand for construction aggregates was expected to rise 5.2% annually to 51.7 billion metric tons [6]. Since the first publication in 1940 by Stanton on the damage of concrete caused by ASR [7], numerous concrete infrastructures such as pavement, bridges, dams and nuclear power plants have been reported to suffer from ASR [8,9]. Taking Switzerland as an example, over 450 concrete structures including 20% of the dam walls have been reported with signs of ASR [10]. Unfortunately, understanding the reaction mechanism and expansion of concrete caused by ASR is challenging, since it is very difficult to isolate a sufficient quantity of phase pure ASR product due to the micro-scale size and tiny amount of these products formed in the veins of concrete aggregates. This difficulty prevented the characterizations of the ASR products with various conventional lab techniques [11].

Recent advanced technologies such as synchrotron-based micro-XRD [12], high pressure XRD [13], micro-Raman spectroscopy [11] and micro-X-ray Absorption Near Edge Structure (XANES) [14] have enabled recording the XRD patterns, Raman spectra and XANES spectra of ASR products directly in situ in the vein of concrete aggregates, which advanced our understanding about the structure and mechanical properties of ASR products. However, the crystal structure and other properties of the ASR products are still unclear due to the limitations of the different techniques. Synthesis of ASR products in larger quantities at 80 °C, at the temperature of the accelerated mortar bar testing methods, has recently been achieved [15]. This allowed characterizations of the synthesized ASR products with a wide range of conventional lab-techniques such as powder XRD, nuclear magnetic resonance (e.g. ^{29}Si MAS NMR), thermogravimetric analysis (TGA), Fourier Transformation-Infrared (FTIR) and dynamic vapor sorption (DVS) [15]. Prediction of the reaction conditions at 80 °C and understanding the role of calcium and/or alkalis together with their combined effects was also made possible based on the developed thermodynamic data for the synthesized ASR products [16,17].

Some studies have shown that the mineralogy of ASR products in field samples can vary from one concrete to another, as reflected by the deviations of the XRD data [18]. On the other hand, Geng et al. [14] showed that for concrete exposed to ambient environment, comparable crystalline ASR products were observed, independent of the source of aggregates, type of cements and countries. Based on the comparison of the results from different studies [12,14,15], it is expected that the variations in the mineralogy of these ASR products may be partially related to the different formation temperatures. Due to the slow formation of ASR product in field concrete, which can take years or decades, the reactivity of aggregates is determined by different accelerated testing methods at elevated temperatures, e.g. accelerated mortar bar test at 80 °C, concrete prism tests (CPT) at 38 and 60 °C [1,19]. Therefore, it is essential to compare and characterize ASR products synthesized at different temperatures.

The occurrence of ASR and the resulting expansion are highly related to the presence of sufficient moisture. Relative humidity (RH) above 80% seems to be required for developing ASR, as discussed by Larive et al. [20]. The internal RH is sufficiently high for ordinary Portland cement concretes with water/cement ratio ≥ 0.45 to produce ASR expansion. At lower water/cement ratio, Lindgård et al. [21] reported that the low RH and low diffusion rate of alkali ions can reduce ASR expansion in concrete. Multon and Toutlemonde [22] investigated ASR expansions of concrete exposed to different RH, and showed, with later water supply, renewed expansions of ASR affected concrete. They attributed this observation to two aspects: (i) ASR products already there can rapidly swell after absorbing water; (ii) ASR formation, which has been stopped by the lack of water, was re-initiated upon water supply. Many studies assumed that ASR products swell after absorbing water, which causes the observed expansion [8,23,24]. However, our understandings of moisture effects on ASR and in particular on its expansion are not sufficient, since it is difficult to directly monitor the changes in quantity and structure of ASR products in concrete under different moisture conditions. Our recent study on synthesized ASR products (both crystalline and amorphous) at 80 °C suggests that swelling by uptake of water is not responsible for expansion caused by ASR products formed at this temperature [15]. However, the moisture stability of ASR products formed at lower temperatures is still unclear.

Taking advantages of our recent experiences and knowledge from the synthesis of the ASR products at 80 °C [15–17], ASR products were synthesized at 40 °C in this study in order to get better understanding of the structure, expansion behavior and formation conditions of ASR products formed in field concrete. For comparison, the data for ASR products formed at 60 and 80 °C and those formed in field concrete at ambient conditions are also re-evaluated.

2. Experimental procedure

2.1. Sample preparation

ASR products containing K as the alkali source were synthesized at 40 °C using the same starting materials and following the same procedure as in the previous study [15]. Two samples with the same initial Ca/Si molar ratio of 0.25 and K/Si molar ratio of 0.5 (i.e. $CaO/SiO_2 = 0.25$ and $K_2O/SiO_2 = 0.25$) were prepared for shorter and longer storage time in case shorter reaction time would not be sufficient. These values were selected since initial Ca/Si ratio in the range 0.1–0.3 and alkali/Si ratio in the range 0.25–0.5 are optimum conditions for synthesizing ASR products according to our recent work conducted at 80 °C [16,17]. The samples were prepared by mixing 6.008 g of hydrophilic silica (SiO_2, specific surface area 200 m^2/g, from EVONIK industries) with 1.402 g of freshly burnt CaO (obtained by burning calcium carbonate for 12 h at 1000 °C), 2.805 g of analytical KOH (≥85% KOH basis) and 50 mL Milli-Q water in 100 mL hard polyethylene (PE-HD) bottles. Each time for the synthesis, freshly burnt CaO was used in order to avoid any potential carbonation of the material. KOH was selected as alkali source since most cements contain more K_2O than Na_2O. After storage at 40 °C for 160 days and 210 days, the samples were filtrated using paper filters with mesh size of 20 μm. The obtained solids were stored in N_2-filled desiccators with a CO_2 absorbent to minimize carbonation and dried prior to analysis using different drying methods, i.e., drying at 35% RH, heating at 80 °C or 110 °C, vacuum drying at 0.03 ± 0.01 mbar depending on the test methods.

For comparison, the data from previous studies for the ASR products synthesized at 80 °C [15] and those formed in field concrete [11,12] and laboratory concrete at 60 °C [15] are re-evaluated. The detailed descriptions of the samples used in this study are summarized in Table 1.

2.2. Analytical methods

The powder X-ray diffraction (XRD, PANalytical X'pert Pro) with CoKα radiation in a θ–θ configuration was used to analyze the synthesized ASR product with a step size of 0.017° 2θ between 5 and 90° 2θ for 2.5 h. Raman spectra were measured with a Bruker Senterra instrument and operated with the software Opus 6.5. The wavelength of the used laser was 532 nm operated at 20 mW. Secondary electron images of the carbon-coated samples were collected using a scanning electron microscope with energy-dispersive X-ray spectroscopy (SEM/EDS) FEI Quanta 650 with an Everhart Thornley Detector. An acceleration voltage of 5 kV and a spot size 2 were used for imaging, and a voltage of 12 and a spot size 4 were used for EDS point analysis. Thermogravimetric

Table 1
The samples used in this study.

Sample names	Descriptions of the different ASR products
Mels_A & Mels_B	Two types of crystalline ASR products with d-spacing of 10.8 Å (Mels_A) and 12.0 Å (Mels_B) corresponding to their first XRD peaks were found in the aggregates of a 50 year old bridge in Mels, Switzerland [11,12,15].
SKC_40 °C_160d	ASR product synthesized at 40 °C after 160 days of reaction
SKC_40 °C_210d	ASR product synthesized at 40 °C after 210 days of reaction
CPT_60 °C	ASR product formed in concrete aggregates during the concrete prism test (CPT) performed at 60 °C [15,41].
SKC_80 °C	ASR product (i.e., K-shlykovite: $KCaSi_4O_8(OH)_3 \cdot 2H_2O$ with a basal spacing of 13.1 Å) synthesized at 80 °C after 80 days of reaction [15].

analysis (TGA) was done with a Mettler Toledo TGA/SDTA 8513 on 10 to 30 mg samples using a heating rate of 20 °C/min from 30 to 980 °C. Dynamic vapor sorption (DVS) was performed on approximately 0.3 g samples within the full range of relative humidity (RH) from 3% to 94% of the instrument. The measurement was started at equilibrium 35% RH and then the sample was subjected to a stepwise absorption and then desorption process. Each RH step was maintained until moisture equilibrium was reached; the equilibrium criterion was a mass change of 0.002% per 5 min. The ^{29}Si MAS NMR experiments were recorded on a Bruker AVANCE III NMR spectrometer using a 7 mm CP/MAS probe at 79.5 MHz applying the same parameters used in the previous study [15]. The ^{29}Si NMR chemical shifts were externally referenced to tetramethylsilane (TMS) at 0.0 ppm.

3. Results and discussion

3.1. ASR product synthesized at 40 °C

The powder XRD patterns of the two synthesized samples dried at 35% RH after reaction times of 160 and 210 days are shown in Fig. 1. Crystalline products with a d-spacing of 10.8 Å at 9.4° 2θ angle are formed in these two samples. The XRD reflections of the two

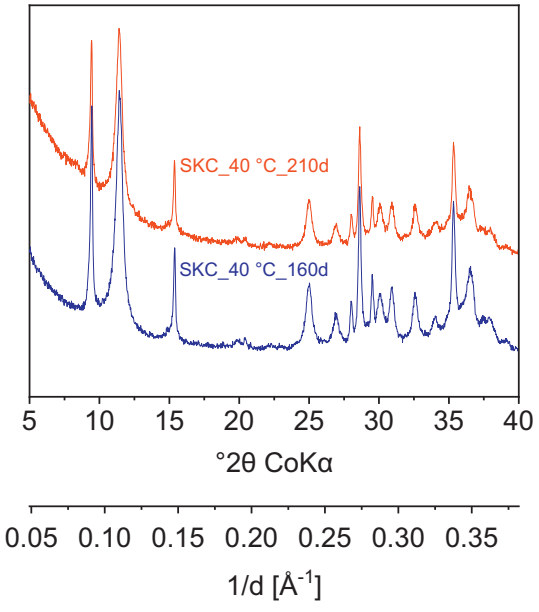

Fig. 1. Powder XRD patterns of the ASR products synthesized at 40 °C after reaction times of 160 and 210 days. The samples were dried at 35% RH prior to the XRD measurements.

synthesized ASR products match very well, indicating that the crystalline ASR product can be reproduced at 40 °C. The possible crystal structure of the 10.8 Å ASR product formed in concrete vein has been recently presented by Dähn et al. [12] based on an in situ measurement using synchrotron-based micro-XRD of the ASR product formed in a concrete aggregate. The presented crystal structure had a layered (Si,O)-framework, forming wide channels and large interlayer spaces filled with cations and water molecules. This structure was closely related to a deformed rhodesite structure, which has also been proposed earlier by de Ceukelaire [25]. However, the main Raman shift for rhodesite is observed between 400 and 500 cm^{-1} [26], which is completely different from the Raman spectra of all types of ASR products, as shown in previous studies [11,15]. Further investigations of the structure of the 10.8 Å ASR product by synchrotron XRD are ongoing.

3.2. Identification of 10.8 Å ASR products in field concrete

Crystalline ASR products with a d-spacing about 10.8 Å at 9.4° 2θ angle has also been observed in field concretes [9,12,15,27–29]. The XRD patterns of the lab-synthesized ASR product are directly compared to those formed in field concrete in Fig. 2a. For the ASR product formed in field concretes, the data obtained from synchrotron-based micro-XRD measurements for ASR products formed in an intact vein in a concrete aggregate is used (Mels_A), where no contaminations of the ASR product by other crystalline solids (e.g. calcite) are expected [12]. The results show that all the XRD peaks of the field ASR product can be found in the powder XRD pattern of the lab-synthesized ASR product (SKC_40 °C_160d). This suggests that the ASR product formed in the vein of aggregate in the field concrete is structurally identical to the ASR product synthesized in the laboratory at 40 °C. However, some differences in the relative intensities of the XRD peaks are observed between the lab-synthesized ASR product and the ASR product formed in field concrete. In addition, the peaks of the powder XRD pattern of the lab-synthesized ASR have a lower full-width at half-maximum (FWHM), and their peaks at higher angles (25–40° 2θ) are much better resolved than the synchrotron-based micro-XRD. For the lab-synthesized ASR product, a powdered sample was used for the XRD measurement, in which the crystals of the ASR product were randomly oriented. No spatial restriction was applied during the synthesis, such that crystals could grow freely. In contrast, on the field ASR product micro-XRD was directly performed on a thin section of a concrete sample, where the crystalline ASR products were formed within a spatially restricted vein in the concrete aggregates, which might limit the crystallite size and result in stacking faults. It is well known that reducing the crystallite size and/or increasing the stacking faults lead to broadening of the XRD peaks [30,31]. In particular, the crystallite size broadening is most pronounced at high 2θ angles based on the Scherrer Equation [31]: $FWHM\,(2\theta) = (K\lambda / L\cos\theta)$, where K is a dimensionless shape factor, λ is the X-ray wavelength and L is the crystallite size.

The strong similarity between the lab-synthesized ASR product (SKC_40 °C_160d) and the ASR product formed in concrete (Mels_A) is supported by comparing their Raman spectra shown in Fig. 2b. Complete peak assignments of the Raman spectra for different types of ASR products are summarized in [15]. The results in Fig. 2b show that nearly identical Raman spectra are observed in the field and synthesized ASR products. The results suggest the presence of silicate sheet structure in the ASR products of both samples, as indicated by the presence of symmetrical bending (600 cm^{-1}) and symmetrical stretching (1115 cm^{-1}) assigned to Q^3 Si-tetrahedra. Moreover, the vibrations involving Ca—O polyhedra (200–350 cm^{-1}) indicate also a strong similarity of their calcium environment in the crystal structure. The limited differences in the relative intensity of the two Raman spectra is likely associated with the surface roughness of the tested samples, as micro-Raman was directly performed on the polished section of the concrete sample, whereas the same measurement was performed on powdered samples for the lab-synthesized ASR product.

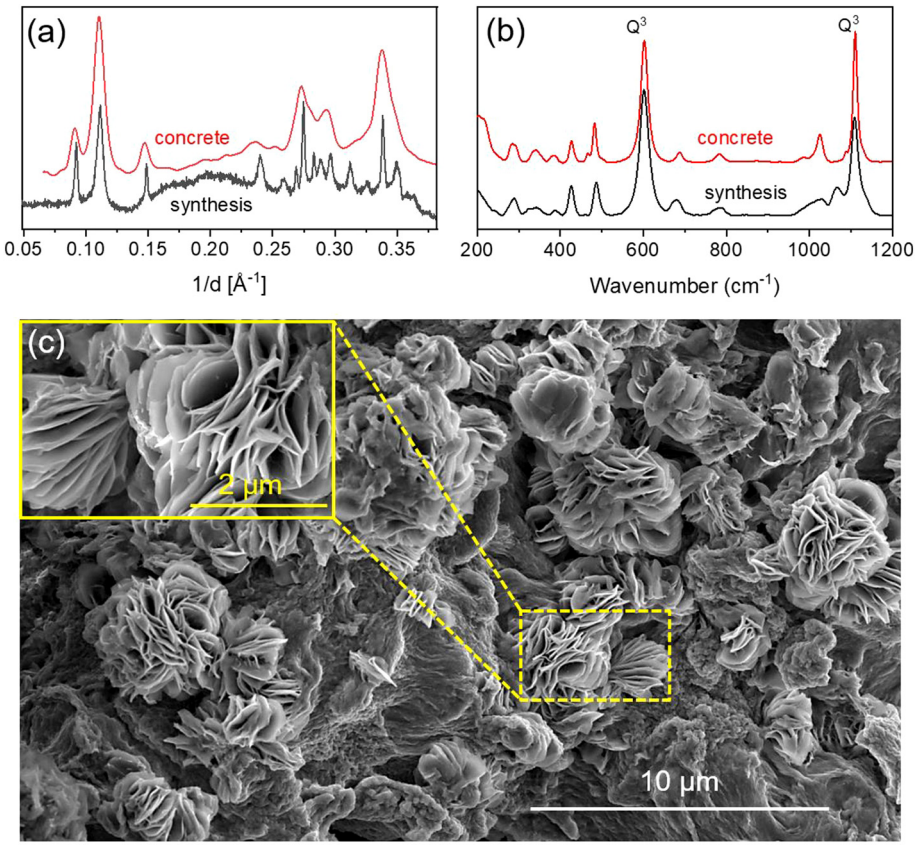

Fig. 2. Comparison of the 10.8 Å ASR products formed in a 50-year old concrete (Mels_A) with that synthesized at 40 °C after reaction time of 160 days (SKC_40 °C_160d): (a) XRD patterns; (b) Micro-Raman spectra; and (c) SEM image of the synthesized 10.8 Å ASR product. The synthesized 10.8 Å ASR product was dried at 35% RH prior to the SEM and Micro-Raman measurements, while it remained in wet condition for the XRD measurement. The data for the concrete samples is reproduced from the previous studies [12,15].

The morphology of the synthesized ASR product after reaction of 160 days is obtained from SEM measurements on the powdered sample dried at 35% RH, as shown in Fig. 2c. A rosette type or plate-like morphology is observed for the crystalline ASR product. Besides, some amorphous reaction products (mainly C-S-H) are also observed in SEM, which are not detected with XRD, likely due to their low amount and amorphous nature. The same plate-like morphology has also been observed in many ASR affected mortars and concretes [25,27,32–38], which also suggests a strong consistency between the synthesized ASR product and that formed in concrete.

The chemical composition of the synthesized crystalline ASR product is obtained from SEM/EDS measurements on the epoxy-impregnated sample after a reaction time of 210 days (SKC_40 °C_210d). The SEM images of the polished section indicate a homogenous crystalline ASR product, which enables the analysis of the chemical composition the obtained crystalline ASR product. The obtained Ca/Si (or CaO/SiO_2) ratio of 0.22 ± 0.01 and K/Si ratio of 0.20 ± 0.03 (i.e. $K_2O/SiO_2 = 0.10 \pm 0.02$) are comparable to the ASR product formed in concrete ($Ca/Si = 0.23 \pm 0.03$; $(K + Na)/Si = 0.22 \pm 0.02$), although some Na is also present in the concrete samples [12].

3.3. Influence of drying on the synthesized 10.8 Å ASR product

The XRD patterns of the synthesized ASR products in wet, 35% RH and vacuum-dried conditions are shown in Fig. 3a. Except for the change of background due to the use of Kapton foil to prevent evaporation of water for the wet sample, no intrinsic difference on the XRD reflections is seen for the samples dried at 35% RH and in wet conditions. The absence of any peak shifts when increasing the RH from 35% to the wet state reveals that no alteration of the structure and volume has occurred. Thus, no expansion of the synthesized ASR product is expected. Significant changes of the XRD reflections, however, are observed when the sample is dried under vacuum; while the first peak (possibly related to the basal spacing) remains similar. There is a clear shift of the second peak at 11.6° 2θ (d = 8.8 Å) to 13.5° 2θ (d = 7.6 Å). The change of crystal structure under such extreme drying conditions, i.e., under vacuum, which does normally not occur in concrete, may help to understand better the structure of the 10.8 Å ASR product.

The vacuum-dried sample was also continuously monitored by XRD during rewetting back to the wet state, see Fig. 3b. Starting from the vacuum-dried condition (curve a), a change of the XRD pattern is observed after storage (in a sealed plastic bag) in a desiccator at 35% RH for nearly 2 months (curve b). A delay of the measurements by 2.5 h (curve b′) and 5 h (curve b″) on the same sample, during which the sample was exposed to air with a RH relatively higher than 50%, shows a further increase of the intensity of the peaks at 11.6° and 15.5° 2θ, and then remains constant. The results shown in Fig. 3 indicate a reversible structural change of the 10.8 Å ASR product upon wetting and vacuum drying. This is again confirmed by repeating the vacuum drying of the same sample without unloading it from the sample holder for 2 days (curve c), which slightly reduced the peak intensity at 11.5° 2θ, indicating that the "loosely bound water" (see DTG curve in later section for this definition) is partially removed.

The SEM images in Fig. 2c show the presence of only one type of crystal with rosette-type or plate-like morphology in the sample (SKC_40 °C_160d) dried at 35% RH. It can be expected that the change of crystal structure upon vacuum drying may result in a change of morphology of the ASR product. The SEM image obtained for the vacuum-dried sample in Fig. 3c shows in addition to the typical rosette or plate-like morphology, ASR products with narrower plate-like and even rod-like morphologies. It should be noted that the vacuum-dried sample can absorb some water from the environment during the

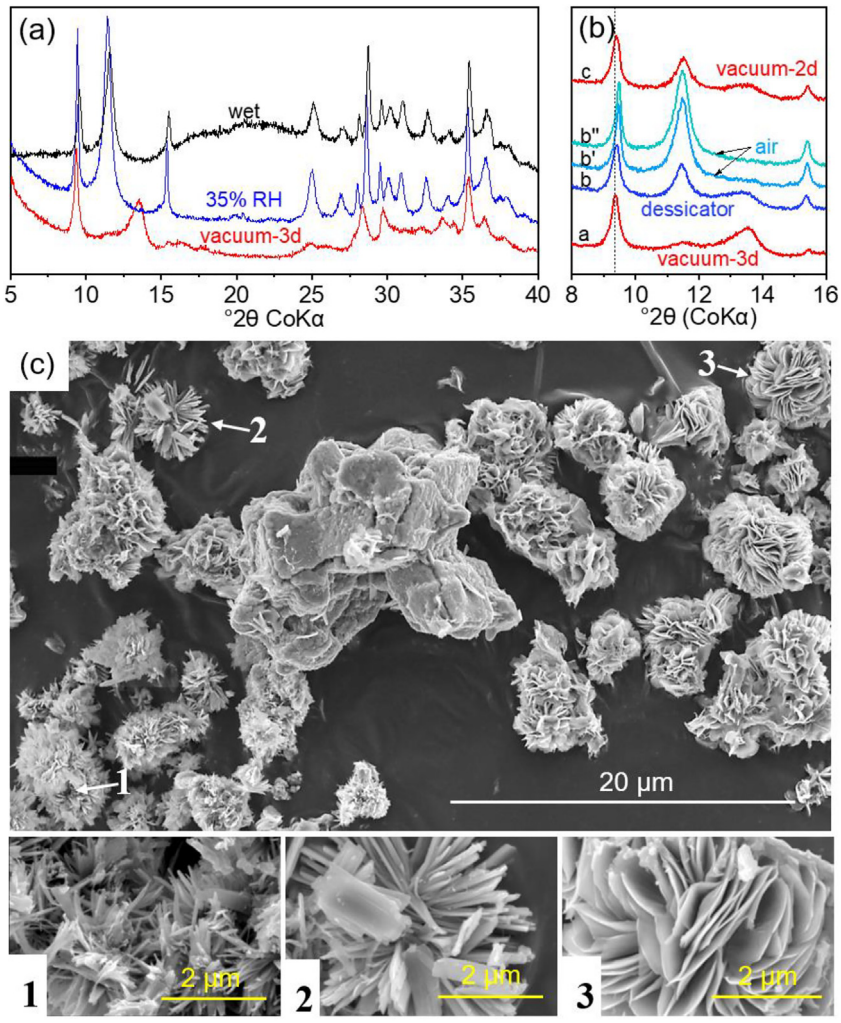

Fig. 3. Effect of different drying conditions and drying history on the synthesized 10.8 Å ASR product (SKC_40 °C_160d): (a) XRD patterns of the three samples dried at different conditions; (b) XRD patterns recorded continuously on one single sample initially vacuum dried for 3 days (curve a). The curve b is recorded directly after taking out the sample from the desiccator; the curves b′ and b″ were recorded immediately on the same sample after recording the curve b, during which the sample was exposed to air; the curve c was recorded after 2 days of re-drying the same sample under vacuum; and (c) SEM images (rod-like "1" and plate-like "2, 3") of the sample after vacuum drying for 3 days.

sample delivery and instrument setup for SEM measurement. Thus, it is not surprising that also the conventional rosette type morphology is observed in the vacuum dried sample. It is not feasible to capture to which extent the change in morphology leads a change of crystal structure, as the uptake of moisture from the air by the synthesized ASR product is very fast. Therefore, a more sophisticated in-situ experiment, which allows recording both morphology and crystal information under the controlled drying conditions, would be needed.

The effect of moisture conditions on the structural change of the synthesized ASR product is also investigated with dynamic vapor sorption (DVS), by monitoring the change of the water absorption and desorption after changing the RH from 3% to 94% over two cycles as shown in Fig. 4a. Overall, no abrupt changes of the sorption and desorption isotherm are observed within the whole range of RH, which tentatively indicates that even drying at 3% RH is probably not harsh enough to alter the crystal structure of the synthesized ASR product. The repeated sorption and desorption cycles follow the initial curves, which also strongly supports that no fundamental structure change occurs. Moreover, some hysteresis is observed for this sample during sorption and desorption process. Similar results are also observed from thermogravimetric analysis (TGA) for the samples with similar drying state (at 35% RH), but different drying history (wet and vacuum dried) as shown in Fig. 4b. No change of chemically bound water is observed from the DTG curve (the first derivative of the TGA curve).

In addition to vacuum drying, heating has also been applied without unloading the sample from the sample holder used for the measurements (Fig. 3b). Only a small amount of loosely bound water is removed upon drying at 80 °C for 3 days (curve b), as shown in Fig. 5, much less than for the vacuum-dried sample (curve a). A delay of the measurements by 2.5 h (curve b′) and 5 h (curve b″) shows a gradual uptake of water from the environment by the synthesized ASR product (SKC_40 °C_160d) as indicated by the increased intensity of the peak at 11.6° 2θ. The sample was further dried at 110 °C for 2 days, i.e. at a temperature where the loosely bound water of the synthesized ASR product is lost, as is evident in the TGA results (Fig. 4b). The XRD pattern (curve c) indicates the disappearance of the peaks at 11.6° and 15.5° 2θ and the appearance of a peak at 13.5° 2θ, i.e. the same effect as vacuum drying (curve a). Also the structure change of the ASR product at 110 °C is reversible, as is further supported by measurements delayed by 2.5 and 5 h (curve c′ and c″), as shown in Fig. 5.

3.4. Influence of temperature on the formation of different types of ASR products

Investigation of the crystalline ASR products formed at different temperatures is essential to understand the mineralogical diversty of ASR products formed in concrete and to assess the reliability of the accelerated ASR performance testing methods. For this purpose, the

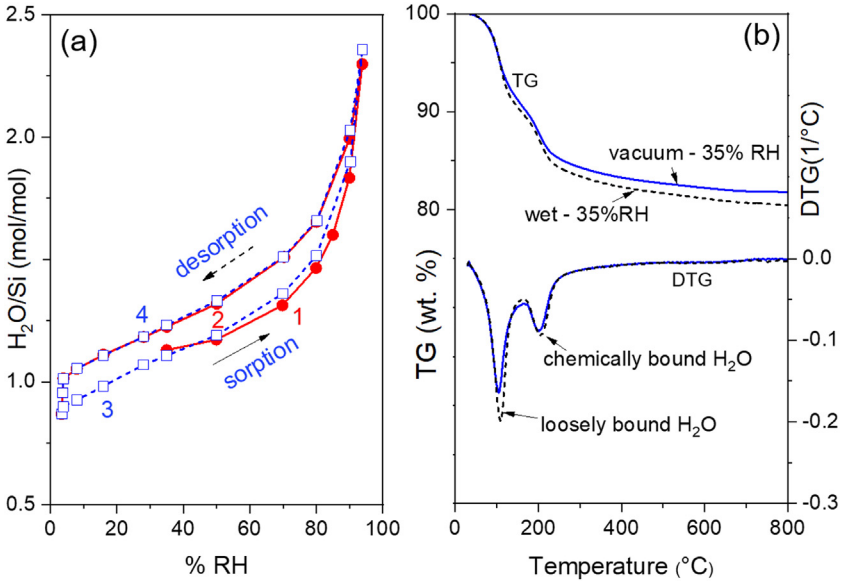

Fig. 4. Change of water content of the synthesized 10.8 Å ASR products (SKC_40 °C_160d) subjected to different drying conditions: (a) sorption and desorption isotherm measured by DVS at RH between 3% and 94%, where the numbers (1–4) indicates the sorption and desorption sequence; and (b) water loss measured by TGA by heating the samples equilibrated at 35%RH but with different initial drying conditions (wet or vacuum for 3 days).

results for a collection of ASR products formed at different temperatures (i.e., ambient, 40, 60 and 80 °C) in laboratory and field concrete are compared for the first time as shown in Fig. 6. Significant differences in the XRD patterns of the ASR products formed at different temperatures are observed (Fig. 6a). The major differences are found in the d-spacing of the first XRD peaks, which are 13.0 Å (80 °C), 10.8 Å (40 °C) and 12.0 Å (at ambient temperature). However, some similar reflections are observed between 0.26 and 0.38 $Å^{-1}$ at all temperatures. These reflections suggests that these ASR products may have some similarities in their short order structures [15], which is further confirmed by the comparable Raman spectra of the ASR products formed at 40, 60 and 80 °C, as shown in Fig. 6b.

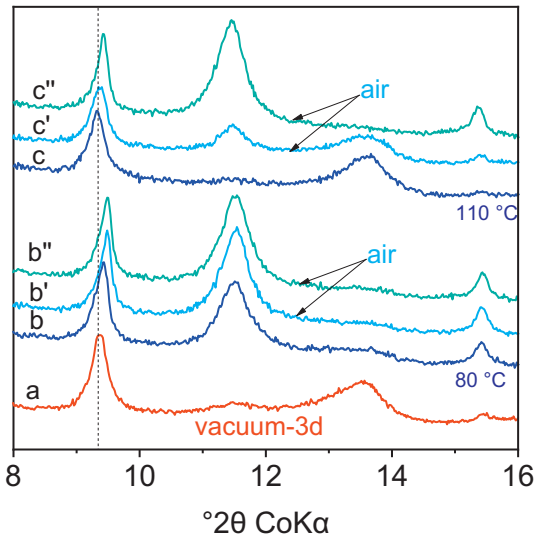

Fig. 5. XRD patterns of the synthesized 10.8 Å ASR product (SKC_40 °C_160d) subjected to heating at 80 and 110 °C for two days prior to the measurements. All the curves were recorded on the same single sample. The curves b and c were recorded after drying the sample at 80 and 110 °C, the curves b′ and b″ were recorded immediately after recording the curve b, similar to the curves c′ and c″ recorded after recording the curve c. During the measurements the sample was exposed to air.

For all types of ASR products formed at different temperatures, Raman spectra in Fig. 6b show the presence of symmetrical bending (600 cm^{-1}) and symmetrical stretching (1115 cm^{-1}) assigned to Q^3 Si-tetrahedra, which indicates the presence of a silicate sheet structure. In particular, the Raman spectra of the ASR products formed at 60 °C and synthesized at 80 °C are identical, namely both of them are 13.1 Å ASR products. The 13.1 Å ASR product was found to be the same as the natural mineral K-shlykovite in terms of its chemical composition and crystal structure [15,39,40]. Some differences in Raman spectra are observed between 13.1 Å (K-shlykovite) and 10.8 Å ASR products, which are consistent with the XRD results as shown in Fig. 6a.

Very few data are available in the literature for the vapor sorption and desorption isotherms of the ASR products. Fig. 6c shows the comparison of the DVS curves of ASR products synthesized at 40 °C (SKC_40 °C_160d) and 80 °C (SKC_80 °C). As a reference, the DVS results for calcium-silicate-hydrate (C-S-H) are also plotted in the same figure. Generally, both ASR products show lower water uptake capacity compared to C-S-H, suggesting that swelling by uptake of water of the investigated ASR products is not responsible for the expansion induced by ASR.

3.5. New insights of the structure of 10.8 Å ASR product from Raman and ^{29}Si MAS NMR data

The structure of crystalline ASR product (13.1 Å) formed at 80 °C has been well explained since it is very similar to the crystal structure of natural K-shlykovite [15,40]. The crystal structure of K-shlykovite is also compatible with the information obtained from powder XRD, ^{29}Si NMR, TGA and Raman spectroscopy [15]. Taking advantages of the large structural similarity between the K-shlykovite and the 10.8 Å ASR product according to Raman spectra (Fig. 6b) and the known structure of K-shlykovite (Fig. 7a), attempts to derive the crystal structure of 10.8 Å ASR product from K-shlykovite have been recently made [14]. By modification of the K-shlykovite structure such as spacing group and unit cell parameters, most of the XRD peaks of the 10.8 Å ASR product could be well fitted. However, two major peaks at 9.5 and 28.7° 2θ could not be well explained, since the atom positions within the Q^3 framework cannot be derived from Raman spectra.

In contrast to Raman, ^{29}Si MAS NMR captures more details of the chemical environment of each Si-tetrahedra within the Q^3 framework.

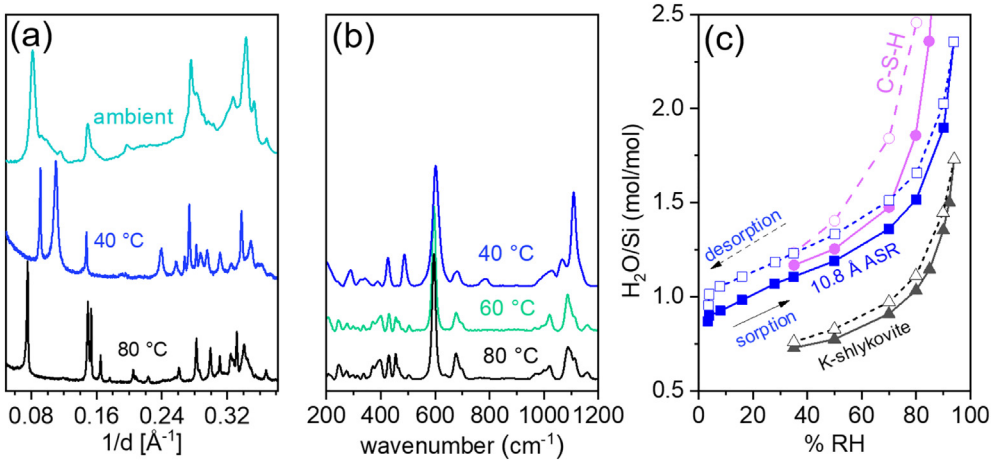

Fig. 6. The different types of ASR products formed at different temperature: (a) XRD patterns for the samples SKC_80 °C (13.1 Å), SKC_40 °C_160d (10.8 Å) and Mels_B (12.1 Å, ambient condition); (b) Raman spectra for the samples SKC_80 °C, CPT_60 °C and SKC_40 °C_160d; and (c) Sorption and desorption isotherm measured by DVS for the samples SKC_80 °C, SKC_40 °C_160d and a reference sample of calcium-silicate-hydrate (C-S-H with Ca/Si ratio of 1.6). The data for the SKC_80 °C, CPT_60 °C and Mels_B are reproduced from a previous study [15]. The data for calcium-silicate-hydrate (C-S-H) is reproduced from another study [42].

In order to trace the possible change of chemical shift related to any structural variations, the ^{29}Si NMR spectra of K-shlykovite (SKC_80 °C) and of 10.8 Å ASR products (SKC_40 °C) dried under vacuum are compared, as shown in Fig. 7b. For all samples, formation of C-S-H as an impurity is observed at chemical shift – 85 ppm. The amount of C-S-H is much lower in the sample (SKC_80 °C) containing K-shlykovite, indicating rather complete conversion of C-S-H to K-shlykovite at 80 °C. At 40 °C, less C-S-H is observed for the SKC_40 °C_210d sample than for the SKC_40 °C_160d sample, indicating conversion of C-S-H to the 10.8 Å ASR product from 160 day to 210 day in the synthetic system. It should be noted that conversion between C-S-H and ASR products can take place in both directions, depending on the starting materials available for the reactions [16,17].

The main resonances related to different types of ASR products are observed between – 90 ppm and–100 ppm. However, significant differences of their relative intensities are also noticed, which indicate some differences in the silicate-sheet structures between K-shlykovite (SKC_80 °C) and 10.8 Å ASR products (SKC_40 °C). For example, the main resonance observed for the K-shlykvoite at −93.8 ppm is attributed to the two Si-tetrahedra sites (Si2 and Si4) which have very similar chemical environment and geometrical symmetry, as shown in Fig. 7a. However, this strong resonance has disappeared for the 10.8 Å ASR, indicating the loss of symmetry of these two Si-tetrahedra. Furthermore, substantial differences in the main resonance between −90 ppm and −100 ppm are also observed for the two 10.8 Å ASR products (SKC_40 °C), which might be related to the uptake of water by the measured samples. Finally, the resonance related to the third Si-tetrahedron (Si3) remains consistent between K-shlykovite and two 10.8 Å ASR products. This observation conforms to the fact this Si-tetrahedron (Si3) is not directly associated with the –OH group or water molecules, as shown in Fig. 7a, and is thus probably less affected by vacuum drying.

Overall, in addition to the change of spacing group and symmetry as proposed by Geng et al. [14], a distortion of the 4-ring and 6-ring silicate framework as shown in Fig. 7a is also expected when considering

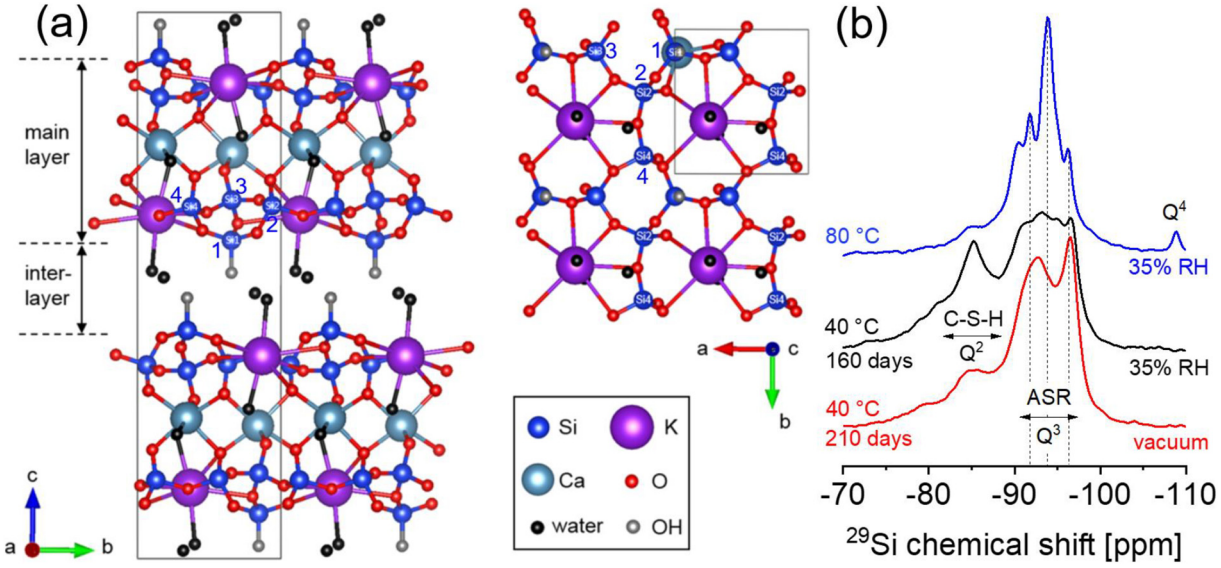

Fig. 7. (a) The crystal structure of K-shlykovite (SKC_80 °C, 13.1 Å = K-shlykovite); and (b) The ^{29}Si NMR spectra of the ASR products synthesized at 40 °C (10.8 Å) and 80 °C (13.1 Å). All samples were vacuum-dried for 3 days prior to ^{29}Si NMR experiments. The crystal structure and the ^{29}Si NMR spectra of K-shlykovite are reproduced from a previous study [15].

transformation of the crystal structure from K-shlykovite to 10.8 Å ASR product. Some extent of reversible deformation of the 4-ring and 6-ring silicate framework can also be expected after vacuum drying. These results provide a new perspective for the further refinement of the crystal structure for the 10.8 Å ASR product.

4. Conclusions

In this study, a crystalline ASR product with d-spacing of 10.8 Å at 9.4° 2θ angle is synthesized at 40 °C. Comparison of the XRD patterns, Raman spectra, morphology and chemical composition with the ASR product formed in a field concrete strongly suggests that the 10.8 Å ASR products formed in laboratory and field concrete are structurally identical.

The structural change of the 10.8 Å ASR product is reversible under vacuum drying, heating at temperature lower than 80 °C and drying at various RH conditions. Moreover, only vacuum drying at 0.03 ± 0.01 mbar or heating at 110 °C can effectively remove the loosely bound water of the 10.8 Å ASR product. The absence an obvious structural change above 3% relative humidity and a lower relative water uptake than observed for C-S-H suggest that swelling of the studied crystalline ASR product is not the responsible mechanism for the macroscopically-observed expansion in ASR affected structures.

The XRD results show formation of crystalline ASR products with different d-spacing for the first XRD peaks at different temperatures, i.e., 12.0 Å (<40 °C), 10.8 Å (40 °C), and 13.1 Å (60–80 °C for K-shlykovite). In addition, Raman spectra show that the ASR product formed at 60 °C is identical to that formed at 80 °C, indicating the formation of K-shlykovite at these temperatures. All types of crystalline ASR products exhibit a layered silicate-sheet structure according to Raman and ^{29}Si NMR spectra. For the 10.8 Å (this study) and 13.0 Å (shlykovite) ASR products, swelling of the reaction products by uptake of water cannot be the mechanism for causing ASR-induced expansion.

CRediT authorship contribution statement

Zhenguo Shi: Conceptualization, Methodology, Investigation, Data analysis, Writing - original draft, Writing - review & editing. **Andreas Leemann:** Methodology, Investigation, Writing - review & editing. **Daniel Rentsch:** Methodology, Investigation, Writing - review & editing. **Barbara Lothenbach:** Conceptualization, Methodology, Investigation, Writing - review & editing.

Declaration of competing interest

The authors declared that they have no conflicts of interest to this work.

Acknowledgements

The authors would like to thank the SNF Sinergia: Alkali-silica reaction in concrete (ASR), grant number CRSII5_17108. The EMPAPOSTDOCS-II programme has received funding from the European Union's Horizon 2020 research and innovation programme under the Marie Skłodowska-Curie grant agreement number 754364. The NMR hardware was partially granted by the Swiss National Science Foundation (SNSF, grant no. 206021_150638/1). Prof. Jørgen Skibsted is acknowledged for the discussion of the NMR spectra. Dr. Frank Winnefeld and Dr. Guoqing Geng are acknowledged for the discussion of the XRD results and Prof. Pietro Lura for a critical and constructive review of the manuscript.

Data availability

The raw/processed data that support the findings of this study are available from the corresponding author upon reasonable request.

References

[1] J. Lindgård, Ö. Andiç-Çakır, I. Fernandes, T.F. Rønning, M.D.A. Thomas, Alkali–silica reactions (ASR): literature review on parameters influencing laboratory performance testing, Cem. Concr. Res. 42 (2012) 223–243, https://doi.org/10.1016/j.cemconres.2011.10.004.
[2] P. Nixon, I. Sims, Testing aggregates for alkali-reactivity, Mater. Struct. 29 (1996) 323–334, https://doi.org/10.1007/BF02486340.
[3] I. Fernandes, M.A.T.M. Broekmans, P. Nixon, I. Sims, M. dos Anjos Ribeiro, F. Noronha, B. Wigum, Alkali–silica reactivity of some common rock types. A global petrographic atlas, Q. J. Eng. Geol. Hydrogeol. 46 (2013) 215–220, https://doi.org/10.1144/qjegh2012-065.
[4] I. Fernandes, M. dos Anjos Ribeiro, M.A.T.M. Broekmans, I. Sims, Petrographic Atlas: Characterisation of Aggregates Regarding Potential Reactivity to Alkalis: RILEM TC 219-ACS Recommended Guidance AAR-1.2, for Use With the RILEM AAR-1.1 Petrographic Examination Method, Springer, 2016.
[5] D. Min, X. Zhongzi, L. Xianghui, H. Sufen, T. Mingshu, Microstructures of some alkali-silica reactive aggregates in China, Cem. Concr. Res. 26 (1996) 663–668, https://doi.org/10.1016/S0008-8846(96)85001-0.
[6] Freedonia, World Construction Aggregates - Demand and Sales Forecasts, Market Share, Market Size, Market Leaders. Study #: 3389, The Freedonia Group, 2019 390.
[7] T.E. Stanton, Influence of cement and aggregate on concrete expansion, Eng. News Record 1 (1940) 59–61.
[8] F. Rajabipour, E. Giannini, C. Dunant, J.H. Ideker, M.D.A. Thomas, Alkali–silica reaction: current understanding of the reaction mechanisms and the knowledge gaps, Cem. Concr. Res. 76 (2015) 130–146, https://doi.org/10.1016/j.cemconres.2015.05.024.
[9] T. Katayama, Petrographic Study of the Alkali-aggregate Reactions in Concrete, Grad. Sch. Sci. Univ. Tokyo, Dep. Earth Planet. Sci., 2012
[10] V. Jensen, C. Merz, Alkali-aggregate reaction in Norway and Switzerland-survey investigations and structural damage, Proc. 13th ICAAR, Trondheim, Norw 2008, p. 785.
[11] A. Leemann, Raman microscopy of alkali-silica reaction (ASR) products formed in concrete, Cem. Concr. Res. 102 (2017) 41–47, https://doi.org/10.1016/j.cemconres.2017.08.014.
[12] R. Dähn, A. Arakcheeva, P. Schaub, P. Pattison, G. Chapuis, D. Grolimund, E. Wieland, A. Leemann, Application of micro X-ray diffraction to investigate the reaction products formed by the alkali–silica reaction in concrete structures, Cem. Concr. Res. 79 (2016) 49–56, https://doi.org/10.1016/j.cemconres.2015.07.012.
[13] G. Geng, Z. Shi, A. Leemann, K. Glazyrin, A. Kleppe, D. Daisenberger, S. Churakov, B. Lothenbach, R. Dähn, E. Wieland, Mechanical behavior and phase change of alkali-silica-reaction products under hydrostatic compression, Acta Crystallogr. Sect. B. (2019)(under review).
[14] G. Geng, Z. Shi, A. Leemann, C. Borca, T. Huthwelker, K. Glazyrin, I.V. Pekov, S. Churakov, B. Lothenbach, R. Dähn, E. Wieland, Atomistic structure of alkali-silica reaction products refined from X-ray diffraction and micro X-ray absorption data, Cem. Concr. Res. (2020), 105958. https://doi.org/10.1016/j.cemconres.2019.105958.
[15] Z. Shi, G. Geng, A. Leemann, B. Lothenbach, Synthesis, characterization, and water uptake property of alkali-silica reaction products, Cem. Concr. Res. 121 (2019) 58–71, https://doi.org/10.1016/j.cemconres.2019.04.009.
[16] Z. Shi, B. Lothenbach, The role of calcium on the formation of alkali-silica reaction products, Cem. Concr. Res. 126 (2019), 105898. https://doi.org/10.1016/j.cemconres.2019.105898.
[17] Z. Shi, B. Lothenbach, The combined effect of potassium, sodium and calcium on the formation of alkali-silica reaction products, Cem. Concr. Res. 127 (2020), 105914. https://doi.org/10.1016/j.cemconres.2019.105914.
[18] T. Katayama, Late-expansive ASR in a 30-year old PC structure in eastern Japan, Proc. 14th Int. Conf. Alkali-Aggregate React. (ICAAR), Austin, Texas, USA, Pap, 2012.
[19] J.H. Ideker, B.L. East, K.J. Folliard, M.D.A. Thomas, B. Fournier, The current state of the accelerated concrete prism test, Cem. Concr. Res. 40 (2010) 550–555, https://doi.org/10.1016/j.cemconres.2009.08.030.
[20] C. Larive, A. Laplaud, O. Coussy, The role of water in alkali-silica reaction, Proc. 11th ICAAR, 1, 2000, p. 8.
[21] J. Lindgård, E.J. Sellevold, M.D.A. Thomas, B. Pedersen, H. Justnes, T.F. Rønning, Alkali–silica reaction (ASR)—performance testing: influence of specimen pretreatment, exposure conditions and prism size on concrete porosity, moisture state and transport properties, Cem. Concr. Res. 53 (2013) 145–167, https://doi.org/10.1016/j.cemconres.2013.05.020.
[22] S. Multon, F. Toutlemonde, Effect of moisture conditions and transfers on alkali silica reaction damaged structures, Cem. Concr. Res. 40 (2010) 924–934, https://doi.org/10.1016/j.cemconres.2010.01.011.
[23] L. Struble, S. Diamond, Unstable swelling behaviour of alkali silica gels, Cem. Concr. Res. 11 (1981) 611–617, https://doi.org/10.1016/0008-8846(81)90091-0.
[24] E. Garcia-Diaz, J. Riche, D. Bulteel, C. Vernet, Mechanism of damage for the alkali–silica reaction, Cem. Concr. Res. 36 (2006) 395–400, https://doi.org/10.1016/j.cemconres.2005.06.003.
[25] L. De Ceukelaire, The determination of the most common crystalline alkali-silica reaction product, Mater. Struct. 24 (1991) 169–171, https://doi.org/10.1007/BF02472981.
[26] R.L. Frost, A. López, Y. Xi, R. Scholz, L. Souza, C. Lana, The molecular structure of the borate mineral rhodizite (K, Cs) Al4Be4 (B, Be) 12O28–a vibrational spectroscopic study, Spectrochim. Acta A Mol. Biomol. Spectrosc. 128 (2014) 291–294, https://doi.org/10.1016/j.saa.2014.02.036.
[27] K. Peterson, D. Gress, T. Van Dam, L. Sutter, Crystallized alkali-silica gel in concrete from the late 1890s, Cem. Concr. Res. 36 (2006) 1523–1532, https://doi.org/10.1016/j.cemconres.2006.05.017.

[28] W.F. Cole, C. Lancucki, Products formed in an aged concrete the occurrence of okenite, Cem. Concr. Res. 13 (1983) 611–618, https://doi.org/10.1016/0008-8846(83)90049-2.
[29] W.F. Cole, C.J. Lancucki, M.J. Sandy, Products formed in an aged concrete, Cem. Concr. Res. 11 (1981) 443–454, https://doi.org/10.1016/0008-8846(81)90116-2.
[30] J.-M. Kim, H.-T. Chung, Electrochemical characteristics of orthorhombic LiMnO2 with different degrees of stacking faults, J. Power Sources 115 (2003) 125–130, https://doi.org/10.1016/S0378-7753(02)00709-7.
[31] A.L. Patterson, The Scherrer formula for X-ray particle size determination, Phys. Rev. 56 (1939) 978, https://doi.org/10.1103/PhysRev.56.978.
[32] T. Katayama, ASR gels and their crystalline phases in concrete—universal products in alkali–silica, alkali–silicate and alkali–carbonate reactions, Proc. 14th Int. Conf. Alkali Aggreg. React. (ICAAR), Austin, Texas 2012, pp. 20–25.
[33] A. Leemann, T. Katayama, I. Fernandes, M.A.T.M. Broekmans, Types of alkali–aggregate reactions and the products formed, Proc. Inst. Civ. Eng. Constr. Mater 169 (2016) 128–135, https://doi.org/10.1680/jcoma.15.00059.
[34] Z. Shi, C. Shi, S. Wan, Z. Zhang, Effects of alkali dosage and silicate modulus on alkali-silica reaction in alkali-activated slag mortars, Cem. Concr. Res. 111 (2018) 104–115, https://doi.org/10.1016/j.cemconres.2018.06.005.
[35] Z. Shi, C. Shi, J. Zhang, S. Wan, Z. Zhang, Z. Ou, Alkali-silica reaction in waterglass-activated slag mortars incorporating fly ash and metakaolin, Cem. Concr. Res. 108 (2018) 10–19, https://doi.org/10.1016/j.cemconres.2018.03.002.
[36] L. Turanli, F. Bektas, P.J.M. Monteiro, Use of ground clay brick as a pozzolanic material to reduce the alkali–silica reaction, Cem. Concr. Res. 33 (2003) 1539–1542, https://doi.org/10.1016/S0008-8846(03)00101-7.
[37] K. Ramyar, O. Çopuroğlu, Ö. Andiç, A.L.A. Fraaij, Comparison of alkali–silica reaction products of fly-ash-or lithium-salt-bearing mortar under long-term accelerated curing, Cem. Concr. Res. 34 (2004) 1179–1183, https://doi.org/10.1016/j.cemconres.2003.12.007.
[38] A. Leemann, I. Borchers, M. Shakoorioskooie, M. Griffa, C. Müller, P. Lura, Microstructural analysis of ASR in concrete - accelerated testing versus natural exposure, Proc. Int. Conf. Sustain. Mater. Syst. Struct. (SMSS2019). Durability, Monit. Repair Struct, Rilem Publications, Paris 2019, pp. 222–229.
[39] I.V. Pekov, N.V. Zubkova, Y.E. Filinchuk, N.V. Chukanov, A.E. Zadov, D.Y. Pushcharovsky, E.R. Gobechiya, Shlykovite KCa [Si4O9(OH)]·3H2O and cryptophyllite K2Ca[Si4O10]·5H2O, new mineral species from the Khibiny alkaline pluton, Kola peninsula, Russia, Geol. Ore Deposits 52 (2010) 767–777, https://doi.org/10.1134/S1075701510080088.
[40] N.V. Zubkova, Y.E. Filinchuk, I.V. Pekov, D.Y. Pushcharovsky, E.R. Gobechiya, Crystal structures of shlykovite and cryptophyllite: comparative crystal chemistry of phyllosilicate minerals of the mountainite family, Eur. J. Mineral. 22 (2010) 547–555, https://doi.org/10.1127/0935-1221/2010/0022-2041.
[41] A. Leemann, The influence of lithium on the structure of ASR products in concrete, Proc. 15th Int. Conf. Alkali-Aggregate React. (15th ICAAR), São Paulo, Brazil, 2016.
[42] E. L'Hôpital, B. Lothenbach, D.A. Kulik, K. Scrivener, Influence of calcium to silica ratio on aluminium uptake in calcium silicate hydrate, Cem. Concr. Res. 85 (2016) 111–121, https://doi.org/10.1016/j.cemconres.2016.01.014.